Contrib Mineral Petrol (2003) 145: 444–459
DOI 10.1007/s00410-003-0451-4

ORIGINAL PAPER

**Jorge Plá Cid · Lauro Valentim Stoll Nardi
Larissa Zitto Stabel · Rômmulo Vieira Conceição
Naira Maria Balzaretti**

High-pressure minerals in mafic microgranular enclaves: evidences for co-mingling between lamprophyric and syenitic magmas at mantle conditions

Received: 11 April 2002 / Accepted: 20 December 2002 / Published online: 20 May 2003

Abstract Mafic microgranular enclaves, composed of diopside and rare magnesium biotite phenocrysts in a groundmass of diopside, biotite, apatite, Fe-Ti-oxides, and alkali feldspar, are associated with Neoproterozoic Piquiri potassic syenite in southern Brazil. Co-genetic mica and clinopyroxene cumulates present inclusions of pyrope-rich garnet in diopside phenocrysts. Textural evidence, as well as the chemical and mineralogical composition, suggest that enclaves crystallized from a lamprophyric magma and co-mingled with the host syenitic magma. The contrasting temperature between both magmas and the consequent chilling was important for the preservation of some early-crystallized minerals in the mafic magma. Diopside groundmass grains contain micro-inclusions of K-rich augite and phlogopite, and some clinopyroxene phenocrysts and elongate groundmass crystals have potassium-rich cores. The pyrope-rich garnet have high #mg number (67–68), with appreciable amounts of Na_2O and K_2O comparable to pyrope synthesized at 5 GPa. The extremely high K_2O contents of K-rich augite micro-inclusions suggest non-equilibrium with the parental magma, whereas the other K-rich clinopyroxenes are similar to K-clinopyroxenes produced at 5–6 GPa. K-clinopyroxene and garnet in mafic microgranular enclaves suggest that lamprophyric magma started its crystallization at upper mantle conditions, and chilled clinopyroxenes with measurable amounts of K_2O are taken as evidence that co-mingling began still at mantle pressures.

J. Plá Cid (✉) · L. V. S. Nardi · L. Z. Stabel
Centro de Estudos em Petrologia e Geoquímica, Instituto de Geociências IGEO/UFRGS, Av. Bento Gonçalves 9500, Campus da Agronomia, CP-15011, 91501-970
Porto Alegre, Brazil
E-mail: placid@bol.com.br

R. V. Conceição · N. M. Balzaretti
Instituto de Física IF/UFRGS. Av. Bento Gonçaves 9500, Campus da Agronomia, CEP-91501-970
Porto Alegre, Brazil

J. Plá Cid
Faculdad de Geologia, Departament de Petrologia, Geoquimica i Prospecciò Geologica, Universidad de Barcelona, Barcelona, Spain

Editorial responsibility: T.L. Grove

Introduction

Numerous papers dealing with K^+ concentration in clinopyroxene were presented in the last three decades, such as Erlank and Kushiro (1970), Harlow and Veblen (1991), Sobolev et al. (1991, 1994), Luth (1992), Edgar and Vukadinovic (1993), Mitchell (1995), Harlow (1996, 1997), Luth (1997), Harlow (1999), and references therein. In all cases, the authors emphasize the importance of very high pressures to admit such a large ion into the pyroxene structure, as well as a K-rich melt. Luth (1997) estimated a minimum of 3 GPa for incorporation of significant amounts of K^+ into clinopyroxene, whereas Erlank and Kushiro (1970) proposed a value of 3.2 GPa. The amount of K admitted into clinopyroxene is also positively correlated with pressure (Luth 1992; Edgar and Vukadinovic 1993; Mitchell 1995; Harlow 1997). The calculated $^{cpx/melt}D_{K2O}$ generally varies from 0.03 to 0.1 (Harlow 1997), reaching up to 0.19 (Edgar and Vukadinovic 1993). The maximum K_2O content found in clinopyroxene is 4.7 wt% (Harlow 1997), from an experimentally produced mixture of 50:50 of diopside and kosmochlor, with K_2CO_3 and $KHCO_3$, at 10 GPa and 1,400 °C. In natural clinopyroxenes included in diamonds, the concentration of K_2O reaches up to 1.5 wt% (Harlow and Veblen 1991). Additionally, K-clinopyroxene was described as inclusions in garnet and zircons from ultrapotassic and ultra high-pressure (UHP) metamorphic rocks (Sobolev et al. 1991, 1994; Collerson et al. 2000). This evidence suggests that K-clinopyroxene is generally an inclusion in mantle refractory phases, which probably prevent its breakdown at lower pressures.

The incorporation of K^+ in the pyroxene structure, as discussed above, is sympathetically related with

increasing pressure. Bukowinski and Knopoff (1977) consider that this element has one-half of its ionic radius at pressures around 50 GPa. The experimental data of Montford and Swanson (1965) confirm the decreasing of ionic volume with increasing pressure. Edgar and Vukadinovic (1993) consider that, in spite of some discrepancies between experimental and theoretical data, the ionic volume of K^+ at 5–6 GPa may be only 80% of that at atmospheric pressure. Calculations effectuated by Harlow (1997), based on the model of Kudoh et al. (1992), show that the ionic volume of K^+ decreases about 30% from ambient conditions to 1,500 °C and 10 GPa.

Several doubts remain with relation to the mechanisms of exchange and charge balance when K^+ is taken into the pyroxene structure. Some discrepancies are observed in the propositions of Harlow and Veblen (1991) and Edgar and Vukadinovic (1993) for coupled exchanges in K-clinopyroxene. However, both agree that the incorporation of trivalent cations in the octahedral site, such as Al^{+3} and Cr^{+3} (Harlow and Veblen 1991) or Fe^{+3} (Edgar and Vukadinovic 1993) is necessary, as well as the replacement of larger ions as Mg^{+2} or Fe^{+2}.

This paper deals with the mineralogical characterization of lamprophyric mafic microgranular enclaves associated with potassic syenites. It emphasizes the occurrence of natural K-clinopyroxenes in these enclaves, as well as pyrope-rich garnet in mica-clinopyroxene cumulates, and discusses its implications for the genesis of potassic silica-saturated magmas under mantle conditions.

The Piquiri Syenite

The Piquiri Syenite, situated in the central part of Rio Grande do Sul state, southern Brazil, is an epizonal intrusion with a crescent shape (Fig. 1) and a diameter of about 12 km. It is related to the post-collisional Neoproterozoic magmatism from southern Brazil (Hartmann et al. 1999; Bitencourt and Nardi 2000), which encompasses: (1) high-K calc-alkaline rocks and peraluminous leucogranites, (2) shoshonitic volcanic and plutonic rocks (Nardi and Lima 1985; Lima and Nardi 1998), and (3) silica-saturated, alkaline volcano-plutonic associations. Their ages are mostly in the range 645–540 Ma, as suggested by Rb–Sr, U–Pb and K–Ar isotope data. The Piquiri Syenite is mainly composed of syenites, quartz syenites and monzonites. This intrusive body is associated with mafic rocks, which occur as microgranular enclaves and cumulates.

The shoshonitic affinity of Piquiri Syenite was suggested by Vieira et al. (1989), and confirmed by its potassic alkaline character ($K_2O + 2 > Na_2O$), and by their mineral composition, according to the criteria proposed by Plá Cid et al. (2000). The major mineral phases are diopside, augite, Mg-hornblende, edenite, magnesian biotite, alkali feldspar, andesine, and apatite, whereas zircon, fluorite, magnetite and ilmenite are the

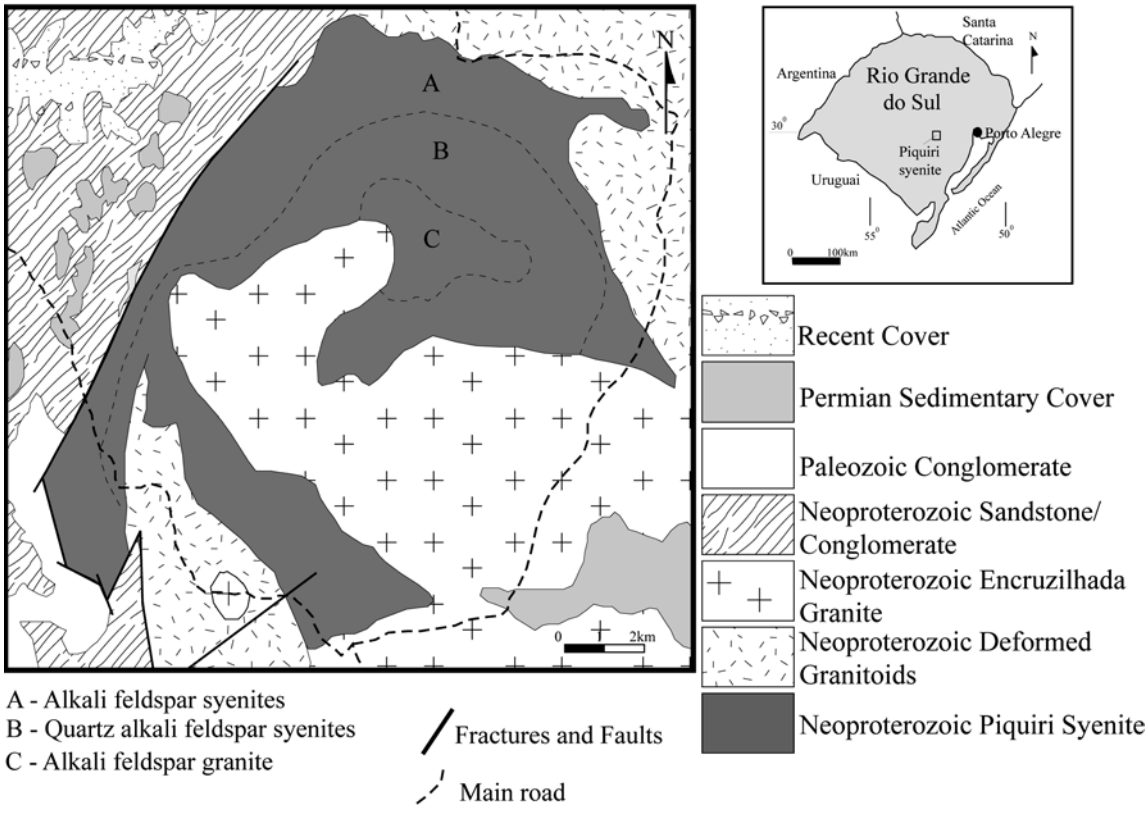

Fig. 1 Piquiri Syenite in the Rio Grande do Sul State, southern Brazil. Modified geological map of Piquiri Syenite, after Vieira et al. (1989)

main accessory phases. Alkali feldspar is generally mesoperthitic with partially resorbed inclusions of plagioclase. The syenite is usually formed by medium-grained and inequigranular rocks, with mineral orientation controlled by magmatic flow. Fine-grained textures are dominant in the border facies, where homogeneous alkali feldspar occurs. Structures, such as *schlieren* and autoliths composed of early mafic phases and apatite are abundant, and reflect the prominent role of magmatic flow during the syenite magma crystallization. The minerals are well preserved, and metamorphic and/or metasomatic effects, as well as solid-state deformation, are not observed.

Enclave types and their relation with the syenite

At least three petrographic types of enclaves were identified: (1) type I—microgranular rocks with dioritic composition and mafic mineralogy constituted by mica, with minor amounts of amphibole, which were interpreted as emplaced into the syenitic intrusion under crustal conditions; (2) type II—mesocratic, fine- to medium-grained inequigranular rocks, with pargasite and aluminous-diopside plus potassium-bearing augite. Only two enclaves of this type were found, and more data are necessary to determine its role in the syenite origin. The alkaline and potassium-rich character of these enclaves suggests that they may be related to the syenite origin, although the absence of chilling textures and the presence of high-pressure minerals do not preclude a xenolithic origin. They are chemically distinguished of type III by lower K_2O/Na_2O ratio, MgO and REE, and higher Al_2O_3, Nb, and U contents; (3) type III—mafic microgranular enclaves (mme) formed by pyroxene and mica phenocrysts, sometimes with microphenocrysts of apatite, in a groundmass made of aciculate and elongate crystals of the same composition, and late-crystallized alkali feldspar. This enclave type is largely dominant ($>90\%$) in the host syenite, and its characterization is the aim of this paper. Their textures indicate that mme are rocks that have the original mineralogy mostly preserved, and the local presence of amphibole rims around clinopyroxene is due to late to post-magmatic transformation by reaction with interstitial water-rich fluid.

The mme have rounded and oval shapes, with diameters between a few centimeters and 2 m. They are widespread in the host syenite, occurring as swarms in the central portion. Close to the contacts with the largest mafic enclaves, the host syenite sometimes presents mesocratic composition. Mme have their mineral components oriented by magmatic flow, and show some internal magmatic orientation of mafic phenocryst. Along the zones where the magmatic flow was more intense, the mme are elongate, frequently disrupted, and associated with *schlieren* and cumulate concentrations of early-crystallized pyroxene and mica, leading to the formation of mesocratic zones.

The contacts between mme and host syenite are generally sharp, irregular and lobate, as generally described for enclaves produced by co-mingling. Chilled margins are rare and were described by Vieira et al. (1989). Most of the petrographic features referred above suggest that co-mingling occurred when both magmas were in a near-liquid state. However, local structures in the mme, such as centimeter-size fractures filled by syenite magma, and the presence of some alkali feldspar xenocrysts, indicate hybridization of the mme during the interaction with the felsic magma. These features suggest that mme from Piquiri Syenite are blobs of coeval magmas, which represent more or less hybridized, mafic end members of a mixing system involving two magmas with contrasting composition, viscosity and temperatures, as described by Vernon (1990) and Didier and Barbarin (1991). Alternative origins for the studied mme, such as autoliths of early-crystallized minerals or xenoliths are completely discarded by the previously described petrographic features and by abundant elongate minerals, which indicate rapid growth in the undercooled mafic magma. Such elongated minerals are formed only by unusually fast temperature decreases, and are not expected in xenoliths or autoliths formed by cumulates of early-crystallized phases.

Cumulates formed by biotite, clinopyroxene, and apatite occur as layers and irregular masses with generally gradational contacts with the host syenite. They are medium grained and equigranular and show the same magmatic-flow orientation of host syenite. They are interpreted as formed by magmatic-flow segregation of syenitic and lamprophyric magmas after mingling and local mixing, and are probably composed mostly of the lamprophyric magma early-crystallized phases.

Petrography of the mme and cumulates

Mafic microgranular enclaves

Mafic microgranular enclaves are black-greenish melanocratic alkali feldspar syenites, according to the modal classification of Le Maitre (1989). They have fine to very fine granulation, with a porphyritic character due to the occurrence of clinopyroxene and more rarely of mica phenocrysts. The major phases are diopside and magnesian biotite, both occurring as phenocrysts and in the groundmass (Fig. 2B). Apatite generally occurs as euhedral, elongate and acicular minerals in the groundmass and, occasionally as micro-phenocrysts. Perthitic alkali feldspar forms poikilitic plates, which include all groundmass minerals. The main accessory minerals are Fe-Ti-oxides, As-Cu-Fe sulphides, zircon, and amphibole. The mineralogical and textural evidences of mme in the Piquiri Syenite indicate a magmatic crystallization with no evidences of metamorphism or sub-solidus transformations.

Clinopyroxene constitutes about 40% of mme mineral components. The mean size of these phenocrysts

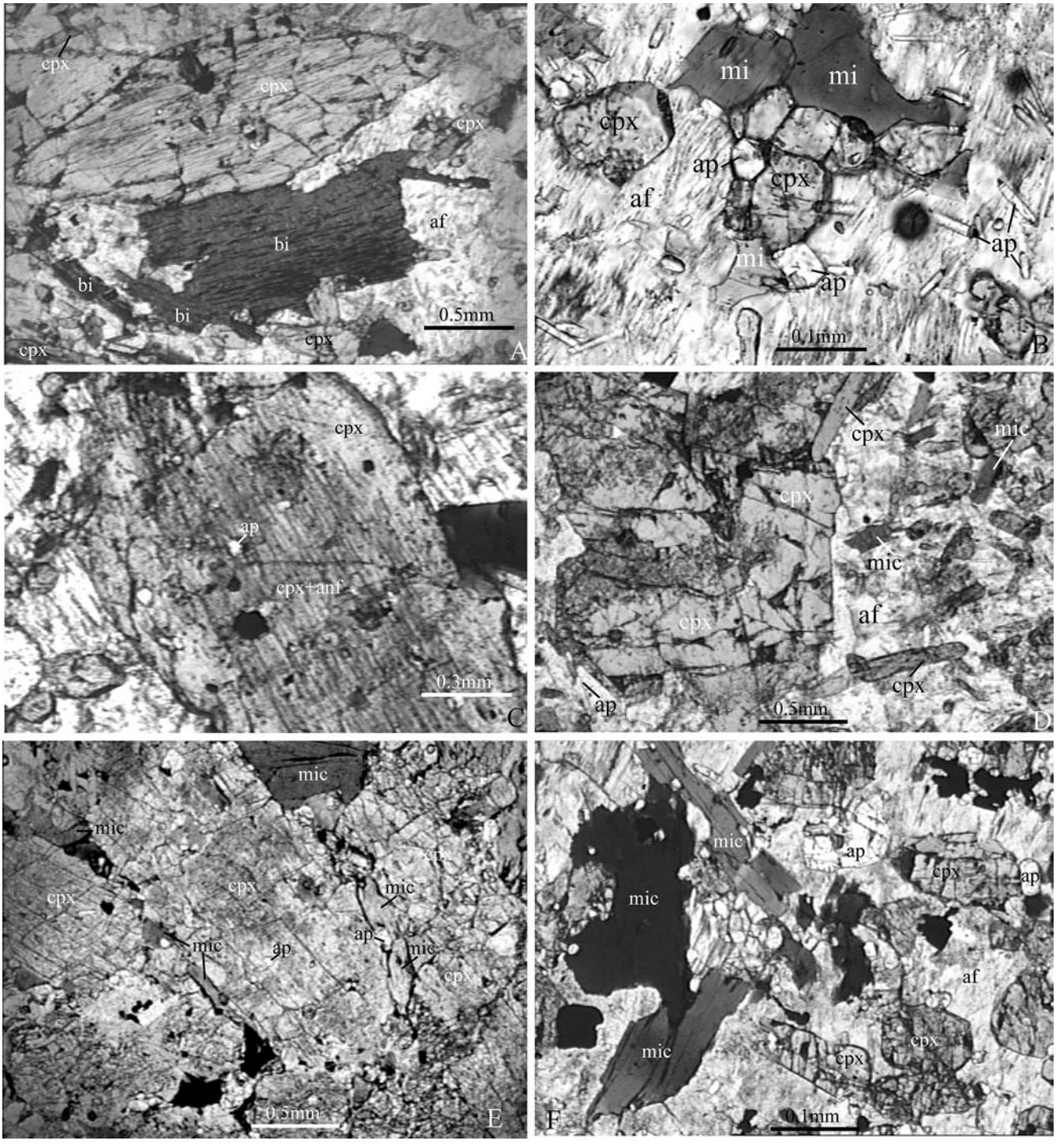

Fig. 2 Digital images under transmitted light obtained by optical microscope showing: **A** clinopyroxene and mica phenocrysts of mme, and elongate clinopyroxene and mica grains engulfed by poikilitic alkali feldspar; **B** two generations of apatite and their relations with groundmass mica and clinopyroxene; **C** zoned clinopyroxene phenocryst, with amphibole lamellae in the core; **D** agglomeration of clinopyroxene phenocrysts without lamellae of amphibole, and at the right side are observed elongate mica and clinopyroxene crystals; **E** clinopyroxene phenocrysts with mica and apatite crystals between them, occurring in the cumulate rocks; **F** alkali feldspar oikocrysts engulfing early crystallized mica, clinopyroxene and apatite in cumulate-rocks

varies from about 2.0 mm long for phenocrysts to 0.25 mm long for groundmass crystals.

Clinopyroxene phenocrysts show green colors, euhedral shape and frequently have lamellae of greenish amphibole in the core. Some phenocrysts are zoned (Fig. 2C). Occasionally clinopyroxene phenocrysts are homogeneous, with no amphibole lamellae (Fig. 2D). Along the clinopyroxene borders, where amphibole lamellae are not observed, occur inclusions of elongate mica. Euhedral and subhedral inclusions of biotite and

phlogopite, euhedral apatite, sulphides and Fe-Ti-oxides are also observed in the clinopyroxene core. Phenocrysts have sharp and non-reactive contacts with the groundmass minerals. Clinopyroxene xenocrysts from the host syenite with *ocelli* texture are sporadically observed.

Groundmass clinopyroxene is pale green and forms euhedral and elongate crystals, frequently with enclosed acicular apatite and mica plates. Fe-Ti-oxides fill the cleavages. In a few samples, clinopyroxene grains are rimmed by bluish amphibole, probably formed by near or sub-solidus interaction with late magmatic fluids.

Phlogopite and biotite reach up to 30% of mme and form light brown, euhedral and elongate grains, and occasionally occur as phenocrysts. They are generally found in the groundmass with the similarly sized pyroxene grains (Fig. 2B). Micas commonly have inclusions of euhedral zircon, Fe-Ti-oxides, and sulphides. Large crystals of brown-reddish, anhedral to subhedral poikilitic biotite, which include acicular and euhedral apatite and pyroxene, are observed in the groundmass. They are formed during the late magmatic stages together with alkali feldspar, under near solidus conditions.

Euhedral and acicular grains of apatite (Fig. 2B) reach up to 4% of the mme. The euhedral grains are early crystallized and occur as inclusions in the mafic phenocrysts. The acicular crystals, sometimes as needles, have the same orientation of the syenite minerals along the contact zone. The form and textural relationship of pyroxene, biotite, and aciculate apatite in the groundmass indicate their simultaneous crystallization.

Alkali feldspar constitutes up to 20% of mme. Perthitic alkali feldspar occurs as poikilitic grains, including the early minerals. Alkali feldspar is sporadically euhedral and homogeneous. Perthitic alkali feldspar phenocrysts sometimes form glomeroporphyrytic texture and are occasionally interpreted as xenocrysts, rimmed by albite, with a size around 2.0 mm. According to Hibbard (1981), Vernon (1983, 1990; 1991), and Barbarin (1988, 1990), this feature is commonly developed in mingling systems during hybridization of mafic magmas by accretion of early crystals from the felsic one. The xenocryst rims have several inclusions of fine and elongate grains of pyroxene and biotite, suggesting growth after mingling. A low degree of contamination of most mme is indicated by absence of xenocrysts.

Mafic phenocrysts and the felsic phases restricted to the groundmass is a typical characteristic of lamprophyric rocks (Rock 1984; Bergman 1986). Mica-lamprophyres, with diopside and/or mica phenocrysts engulfed by an alkali feldspar-rich groundmass, have been described as minettes (Rock 1984, 1991; Thompson et al. 1984, 1989; Mitchell and Bergman 1991). The low contamination of the mme, the absence of solid-state transformations, as well as their textural characteristics, lead to their identification with chilled mafic rocks crystallized from minette-like magma, as discussed by Vieira et al. (1989).

Mica-clinopyroxene cumulates

These rocks are compositionally identical to the mme, formed basically by the paragenesis diopside–biotite/phlogopite–apatite. They are black-greenish melanocratic medium- to coarse-grained rocks, with inequigranular texture (Fig. 2B). The mineral constituents of cumulates are similar to the early crystallized phases of mme, which suggests that they are formed from the same mafic magma. Mica-clinopyroxene cumulates contain intercumulus, perthitic, alkali-feldspar oikocrysts, with diameter up to 1 cm, with euhedral inclusions of clinopyroxene, mica, and apatite (Fig. 2F). The mineral composition and crystallization order observed in oikocrysts and mme is exactly the same (Fig. 2A, B, F).

Euhedral clinopyroxene, sometimes with amphibole lamellae and inclusions, as observed in mme, is the main component of mica-clinopyroxene cumulates. These clinopyroxene crystals are optically homogeneous, without evidence of zoning. Euhedral inclusions of apatite, mica, and subhedral, nearly rounded inclusions of garnet, with pale gray-pinkish color, occur in some grains.

Early-crystallized biotite occurs as micro-inclusions in clinopyroxenes. Euhedral brown crystals of mica generally occupy the interstitial regions between clinopyroxene grains. Contacts between these phases are straight, non-reactive, and suggest equilibrium crystallization. Late-crystallized anhedral grains of biotite contain a large amount of acicular apatite.

Apatite is a major constituent of mica-clinopyroxene cumulates and can reach up to 10%. It occurs as euhedral grains uniformly distributed or as inclusions mostly in clinopyroxene.

Fe-Ti-oxides are relatively abundant, occurring either in the interstitial regions between clinopyroxene grains together with mica, or as inclusions in clinopyroxene and mica. Other accessory phases are sulphides and zircon.

Analytical techniques

The chemical compositions of minerals were measured with a CAMECA SX-50 Electron Microprobe, at the Electron Probe Laboratories from Universidade Federal do Rio Grande do Sul, Brazil, and from the Serveis Cientificotècnics of Universitat de Barcelona, Spain.

Backscattered electron (BSE) mineral images of K-clinopyroxene crystals were performed on a JEOL SM-5800 (SEM), at the Microscopic Center from Universidade Federal do Rio Grande do Sul, Brasil. X-ray images of the potassium-rich cores in clinopyroxene were obtained on the electron microprobe at the Universitat de Barcelona.

The CAMECA SX-50 is an electron microprobe with four wavelength dispersion spectrometers. The analytical conditions used were a beam current of 10 nA, beam energy of 15 keV and a spot size of 1 μm. The acquisition time was 20 s on the peak and 10 s on the background for all elements. Each element was standardized on either synthetic or natural minerals. Ferric iron was calculated, considering stoichiometric criteria, by the software accomplished in the electron microprobe, and these data were

checked using the suggestion of Droop (1987), as well as through the software Minpet 2.02. Fluorine in mica and amphibole was analyzed under the same conditions of the other elements, standardized with natural fluorite. K-characteristic x-ray map was obtained using a beam current of 100 nA, and beam energy of 20 keV.

Raman spectra were obtained using a microspectrometer at the High-Pressures Laboratory from Physics Institute, at the Universidade Federal do Rio Grande do Sul. The equipment consists of one Olympus (BH-2 model) microscope, with a simple monochromator (Jobin Yvon; HR-320 model) and one CCD (Charged Coupled Device, EG&G; 1530-C-1024S model) detector refrigerated with liquid nitrogen. The spot size was adjusted to 2 μm. The laser source used as excitation light is of HeNe, with beam energy of 30 mW and wavelength of 632.8 nm.

Mineral composition

Phenocrysts and groundmass clinopyroxenes

Phenocrysts and groundmass crystals are close to the boundary between diopside and augite (Morimoto 1988; Table 1, Fig. 3). Phenocrysts (Fig. 3A) have lower contents of ferrosilite (Fs), ranging from 5.6 to 16.1%, with most data between 12–14%, and higher concentrations of enstatite (En, 36.1–46.2%). The groundmass clinopyroxenes contain 8.2–18.2% Fs and 33.6–41.2% En (Fig. 3A). Clinopyroxenes of mme have #mg between 59 and 80, with the higher values generally in the phenocrysts. The highest En contents are concentrated in the phenocrysts of the mica-clinopyroxene cumulates (Fig. 3A), where #mg varies from 70 to 90. Clinopyroxenes included in alkali feldspar oikocrysts have #mg close to 70. The low amounts of octahedral aluminum in phenocrysts and groundmass crystals lead to low amounts of jadeite (Jd) component in both groups (Table 1). En and Wo components of clinopyroxene included in oikocrysts are closer to those of phenocrysts and of Mg-rich mme crystals. Cr_2O_3 contents are generally below the detection limit. In cumulates, the highest concentration is 0.23 wt%. Phenocrysts of mme have comparable amounts and, for groundmass crystals, Cr_2O_3 ranges between 0.10 and 0.58 wt%.

K-rich clinopyroxenes

Chemical analyses of some groundmass and phenocryst clinopyroxenes show measurable amounts of K_2O (Table 2). In order to check if these potassium concentrations are really incorporated by clinopyroxene, or are due to the presence of ex-solved phases and/or micro-inclusions, several independent techniques were used.

BSE images obtained by electron microscope revealed that the richest potassium compositions (see analyses A

Table 1 Representative analyses (in wt%) of pyroxenes from phenocrysts, groundmass, and cumulates–rocks

	*	*	*	*	*	**	**	**	**	**	***	***
SiO_2	54.29	53.74	54.67	54.11	55.08	53.93	53.78	53.80	53.98	54.32	54.20	54.64
TiO_2	0.42	0.18	0.21	0.50	0.37	0.30	0.31	0.09	0.21	0.21	0.32	0.31
Al_2O_3	0.87	0.43	0.36	0.69	0.84	0.48	0.40	0.44	0.50	0.46	0.50	0.55
FeO	4.50	8.38	7.17	8.49	3.69	8.64	9.22	9.23	10.11	10.01	3.50	2.95
Fe_2O_3	0.37	2.55	1.15	0.77	0.00	2.44	1.75	2.05	1.12	0.49	0.00	0.50
Cr_2O_3	0.00	0.00	0.01	0.00	0.29	0.00	0.00	0.00	0.00	0.00	0.00	0.23
MnO	0.18	0.39	0.31	0.39	0.12	0.42	0.45	0.35	0.35	0.41	0.00	0.12
MgO	15.93	11.95	14.00	13.67	17.10	12.41	12.45	11.63	11.82	12.61	17.02	16.89
CaO	23.93	21.26	22.33	21.36	23.85	20.77	20.71	20.97	20.47	20.88	24.19	24.24
Na_2O	0.34	1.52	0.95	0.97	0.16	1.49	1.31	1.56	1.49	1.18	0.27	0.30
K_2O	0.00	0.00	0.00	0.00	0.00	0.00	0.00	0.00	0.00	0.00	0.00	0.00
Total	100.82	100.41	101.16	100.95	101.52	100.88	100.39	100.12	100.06	100.56	100.00	100.73
Structural formulae based on 6 oxygens												
TSi	1.98	2.01	2.01	2.00	1.98	2.00	2.01	2.02	2.02	2.02	1.98	1.98
TAl	0.02	0.00	0.00	0.01	0.02	0.00	0.00	0.00	0.00	0.00	0.02	0.02
M1Al	0.01	0.02	0.02	0.03	0.02	0.02	0.02	0.02	0.02	0.02	0.00	0.00
M1Ti	0.01	0.01	0.01	0.01	0.01	0.01	0.01	0.00	0.01	0.01	0.01	0.01
M1Fe3	0.01	0.07	0.03	0.02	0.00	0.07	0.05	0.06	0.03	0.01	0.03	0.01
M1Fe2	0.10	0.24	0.18	0.19	0.05	0.22	0.24	0.27	0.28	0.26	0.04	0.06
M1Cr	0.00	0.00	0.00	0.00	0.01	0.00	0.00	0.00	0.00	0.00	0.00	0.01
M1 Mg	0.87	0.67	0.77	0.75	0.92	0.69	0.69	0.65	0.66	0.70	0.93	0.91
M2 Mg	0.00	0.00	0.00	0.00	0.00	0.00	0.00	0.00	0.00	0.00	0.00	0.00
M2Fe2	0.04	0.02	0.04	0.07	0.07	0.05	0.06	0.02	0.04	0.05	0.04	0.03
M2Mn	0.01	0.01	0.01	0.01	0.00	0.01	0.01	0.01	0.01	0.01	0.00	0.00
M2Ca	0.93	0.85	0.88	0.84	0.92	0.83	0.83	0.84	0.82	0.83	0.94	0.94
M2Na	0.02	0.11	0.07	0.07	0.01	0.11	0.10	0.11	0.11	0.09	0.02	0.02
Cation	4.00	4.00	4.00	4.00	4.00	4.00	4.00	4.00	4.00	4.00	4.00	4.00
Jd	1.43	2.09	1.69	2.72	1.81	2.30	1.95	2.09	2.38	2.12	0.00	0.45
Wo	47.53	46.81	46.23	44.21	46.35	45.29	44.81	46.31	44.55	44.16	47.81	48.00
Fs	6.98	14.48	11.74	13.72	5.59	14.80	15.75	15.90	17.29	16.61	5.40	5.44
En	44.07	36.62	40.34	39.34	46.25	37.61	37.50	35.70	35.77	37.10	46.79	46.55

[a]* Phenocrysts; ** groundmass; *** mica–clinopyroxene cumulates

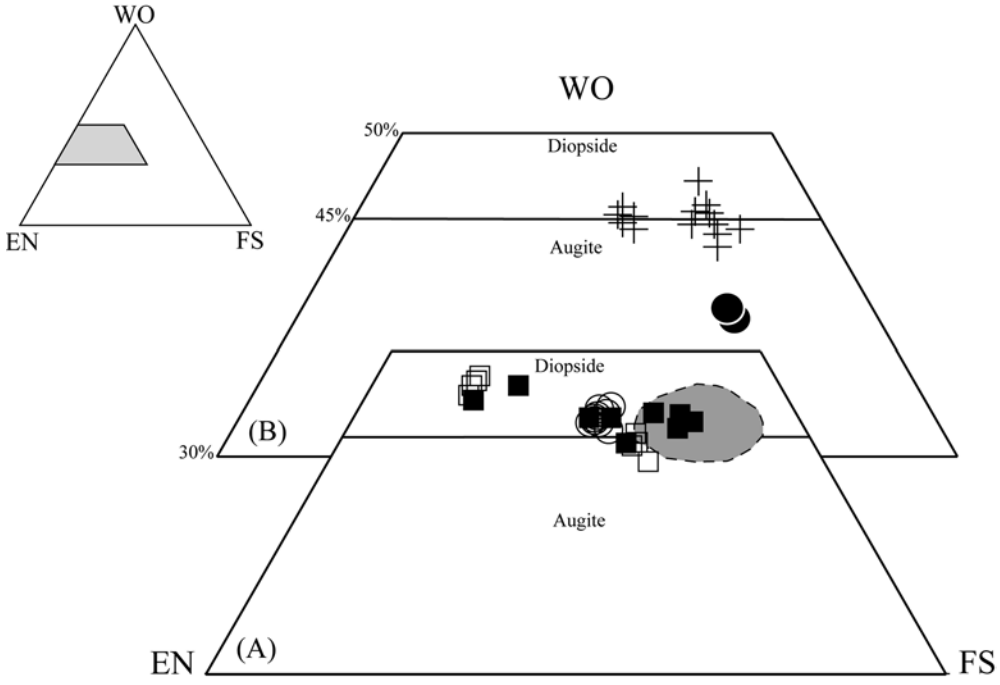

Fig. 3 Wollastonite (*Wo*)–enstatite (*En*)–ferrosilite (*Fs*) classificatory diagram (Morimoto 1988). *A* Shadow area (groundmass crystals); *open squares* (cumulate-rocks phenocrysts); *filled squares* (cumulate-rocks pyroxenes included in oikocrysts); *open circles* (mme phenocrysts). B-crosses (K-clinopyroxenes: phenocrysts and groundmass crystals); filled circles (K-clinopyroxenes micro-inclusions)

and B in Table 2) were in acicular micro-inclusions (Fig. 4A) with a small size that difficult the determination of their optical properties. Attempts to detect F and Cl in these micro-inclusions have failed. Microprobe determinations of Na_2O in micro-inclusions indicate higher contents than those observed on phenocrysts, and nearly the same as those of groundmass crystals (Tables 1 and 2). Additionally, the diopside host of micro-inclusions contains around 1.44 wt% of Na_2O, a similar value to those of micro-inclusions (Fig. 4A). All these chemical evidences indicate these micro-inclusions are clinopyroxenes, and exclude the possibility of being some kind of mica or amphibole. The micro-inclusions of clinopyroxene are Al-rich augite (Al_2O_3 up to 2.07 wt%), and their K_2O contents are unusually high, up to 1.97 wt%, when compared with those of literature (Harlow and Veblen 1991; Luth 1997, and references therein). In order to identify structural patterns of pyroxene in the micro-inclusions, the Raman spectroscopy technique was used. Raman scattering term is used to describe the energy changes suffered by a light beam (i.e., laser) due to inelastic collisions with sample molecules (i.e., a mineral). Each group of molecules of one sample has specific vibration modes, depending on atom types and on its three-dimensioned distribution (McMillan 1989). The Raman active vibrational bands of calcic clinopyroxenes are 389, 665, and 1,011 cm^{-1} (Mernagh and Hoatson 1997; Huang et al. 2000, Wang et al. 2001). All analyzed clinopyroxenes show such characteristic vibrational bands, either in the regions corresponding to the host or micro-inclusions (Fig. 5). In addition, there is a stronger fluorescence in the micro-inclusions than on diopside host and on clinopyroxenes without potassium.

Microprobe analysis has also revealed significative potassium contents in the cores of some elongate groundmass crystals and in the core of some phenocrysts (Table 2). These clinopyroxene phenocrysts do not exhibit amphibole exsolutions in the core, and the elongate grains are light green without evidence of alteration or transformation for hydrated phases such as mica or amphibole. All these clinopyroxenes are on the boundary between augite and diopside (Fig. 3B), and have K_2O concentrations varying from 0.10 to 0.63 wt%. High magnification (×500) in the SEM does not show the presence of inclusions at the studied elongate crystal surface. Characteristic x-ray map for K^+ of its basal section, which contains 0.44 wt% of K_2O in the core (Table 2), shows that the high K_2O contents are limited to the core of the grain (Fig. 4B). The morphology of the K-enriched zone suggests it is not an inclusion.

The K-augite micro-inclusions are characterized by the highest amounts of Ti, Fe^{3+}, and Al among all analyzed K-rich clinopyroxenes. The micro-inclusions and cores of elongate crystals show antipathetic correlation between K^+ and Ca^{2+}, in agreement with the substitutional model suggested by Harlow (1996, 1997), and by the experimental data of Mitchell (1995). In order to balance the K^+ in the M2 site, substitutions in M1 site of larger ions by smaller ones, are necessary (Edgar and Vukadinovic 1993; Harlow 1996, 1997). The negative correlation between Fe^{2+}, and calculated Fe^{3+} + Mg in the M1 site (Fig. 6A) suggests expansion of M2 site for K^+ accommodation. In spite of dependence between Fe^{+2} and calculated Fe^{3+}, this substitution probably occurs, since there are low amounts of other trivalent ions as Cr and Al. A negative correlation of K_2O with Fe^{2+} in some K-clinopyroxene grains

Table 2 Representative analyses of K-clinopyroxene (in wt%) from phenocrysts, groundmass grains, and micro-inclusions. End members: Ticpx ($CaTiAl_2O_6$); Kcpx ($KFe^{3+}Si_2O_6$); Jd ($NaAlSi_2O_6$); Wo ($Ca_2Si_2O_6$); Fs ($Fe_2Si_2O_6$); En ($Mg_2Si_2O_6$); CaTs ($CaAlSi_2O_6$); Ac ($NaFe^{3+}Si_2O_6$)

	Ground	Ground	Ground	Ground	Pheno	Pheno	Pheno	Pheno	Pheno	Micro-A	Micro-B
Sample	1F	205	211[a]	202	211	211	211	211	211	7–10	7–10
SiO_2	51.847	53.264	52.693	53.086	53.410	53.176	53.803	53.536	53.095	50.290	52.230
TiO_2	0.561	0.219	0.370	0.356	0.282	0.338	0.300	0.295	0.374	1.060	0.600
Al_2O_3	1.236	0.618	1.051	0.975	0.548	0.496	0.497	0.549	0.613	2.740	1.890
Cr_2O_3	0.125	0.000	0.107	0.000	0.000	0.000	0.000	0.000	0.000	0.270	0.000
Fe_2O_3	4.376	2.282	3.527	2.681	3.564	4.395	2.339	3.969	3.589	5.270	4.670
MgO	11.115	11.720	11.715	11.719	13.987	13.923	13.936	14.056	12.277	11.370	11.710
CaO	19.740	20.599	19.346	19.766	21.422	21.373	21.710	21.407	20.587	16.300	17.000
MnO	0.355	0.331	0.355	0.387	0.412	0.327	0.135	0.398	0.357	0.300	0.450
FeO	7.900	8.401	8.290	8.529	5.301	4.664	6.455	5.072	7.326	7.650	8.040
Na_2O	1.573	1.582	1.660	1.801	1.063	1.030	1.002	1.025	1.596	1.290	1.410
K_2O	0.605	0.176	0.436	0.104	0.361	0.630	0.235	0.517	0.158	1.970	1.750
Total	99.430	99.190	99.550	99.400	100.350	100.350	100.410	100.820	99.970	98.52	99.74
Structural formulae based on 6 oxygens											
TSi	1.965	2.010	1.986	1.999	1.977	1.970	1.990	1.974	1.987	1.920	1.970
TAl	0.035	0.000	0.014	0.001	0.023	0.022	0.010	0.024	0.013	0.080	0.030
M1Al	0.020	0.027	0.032	0.042	0.001	0.000	0.011	0.000	0.014	0.050	0.050
M1Ti	0.016	0.006	0.010	0.010	0.008	0.009	0.008	0.008	0.011	0.030	0.020
$M1Fe^{+3}$	0.124	0.065	0.100	0.076	0.099	0.106	0.065	0.105	0.101	0.150	0.130
$M1Fe^{+2}$	0.208	0.243	0.196	0.215	0.120	0.115	0.147	0.115	0.190	0.120	0.140
M1Cr	0.004	0.000	0.003	0.000	0.000	0.000	0.000	0.000	0.000	0.010	0.000
M1 Mg	0.628	0.659	0.658	0.658	0.772	0.769	0.768	0.772	0.685	0.650	0.660
$M2Fe^{+2}$	0.042	0.023	0.065	0.054	0.044	0.037	0.053	0.044	0.040	0.130	0.110
M2Mn	0.011	0.011	0.011	0.012	0.013	0.010	0.004	0.012	0.011	0.010	0.010
M2Ca	0.801	0.833	0.781	0.797	0.850	0.848	0.860	0.846	0.826	0.670	0.690
M2Na	0.116	0.116	0.121	0.131	0.076	0.074	0.072	0.073	0.116	0.100	0.100
M2K	0.029	0.008	0.021	0.005	0.017	0.030	0.011	0.024	0.008	0.100	0.080
Cations	3.999	4.001	3.998	4.000	4.000	3.998	3.999	4.000	4.002	4.000	4.000
Ticpx	0.064	0.000	0.028	0.002	0.032	0.036	0.020	0.032	0.026	0.120	0.060
CaTs	0.040	0.054	0.064	0.084	0.003	0.000	0.022	0.000	0.028	0.140	0.130
Wo	0.765	0.806	0.742	0.754	0.841	0.839	0.845	0.838	0.804	0.570	0.610
En	0.628	0.659	0.658	0.658	0.772	0.769	0.768	0.772	0.685	0.650	0.660
Fs	0.106	0.088	0.152	0.132	0.114	0.094	0.114	0.112	0.102	0.240	0.240
Kcpx	0.058	0.016	0.042	0.010	0.034	0.060	0.022	0.048	0.016	0.200	0.160
Jd	0.000	0.000	0.000	0.00	0.000	0.000	0.000	0.000	0.000	0.000	0.000
Ac	0.198	0.114	0.164	0.142	0.152	0.148	0.108	0.146	0.186	0.120	0.100

[a]Chemical analyses of pyroxene core observed in Fig. 4A

(Fig. 6A) confirms the role of substitutional schemes involving the K and Fe. The concomitant incorporation of K^+ and Na^+ in the M2 site is associated to Ca^{2+} + Fe^{2+} depletion (Fig. 6B). In the M2 site, the increase of Na^+ is admitted by Luth (1997), in order to allow substitution of Ca^{2+} by Na^+ + K^+, through an increase in the polyhedral compressibility. Aluminum is preferentially incorporated as ^{IV}Al, since some K-rich clinopyroxenes are silica-deficient (Table 2).

End-member best estimations are shown in Table 2. Ti was accounted in Ticpx component, and the remaining ^{IV}Al together with ^{VI}Al and Ca were used to calculate CaTs. Ferric iron was used to estimate Kcpx component, together with Cr, and the remaining Fe^{+3} was incorporated in determinations of Ac component. Mn was used with Fe^{22} in Fs component. Jd end-member is absent, because all ^{VI}Al is consumed in CaTs component. Micro-inclusions have higher amounts of CaTs and Ticpx than the other K-clinopyroxene crystals, reflecting higher contents of Al_2O_3 and TiO_2. Micro-inclusions, as expected, have also higher Kcpx component, and Kcpx/Ac ratios above 1, which are usually below unity for the other K-clinopyroxene (Table 2). Wo presents the lowest values in micro-inclusions, confirming the negative correlation observed between K and Ca in Fig. 6A.

Mica

According to the nomenclature proposed by Rieder et al. (1998), the mme micas are tri-octahedral types, with composition of Mg-biotite and phlogopite (Fig. 7A). Phlogopite compositions are represented by three analyses of elongate inclusions in diopside groundmass crystals. They have Mg/Mg + Fe ratios up to 0.69, whilst groundmass crystals plot generally in the biotite field with values from 0.58 to 0.66 (Table 3). In some mme mica occurs along fractures of feldspar xenocrysts and shows lower Mg/Mg + Fe (0.46–0.56). Phlogopite is Al enriched (Table 3), with about 2.11 apfu, while most Mg-biotite show values around 2

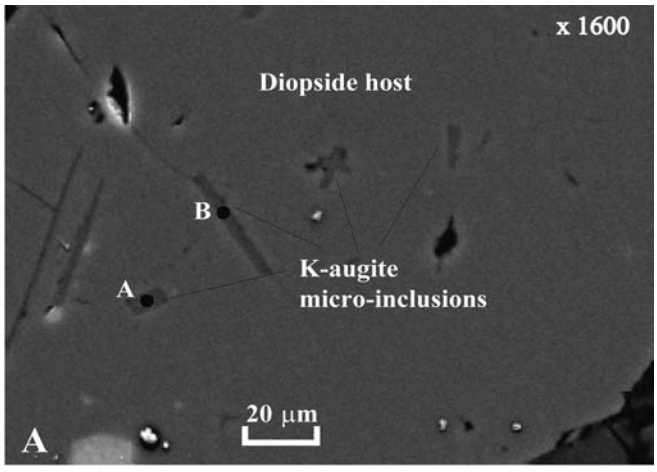

A - K_2O (1.97wt%); Na_2O (1.29wt%)
B - K_2O (1.75wt%); Na_2O (1.41wt%)

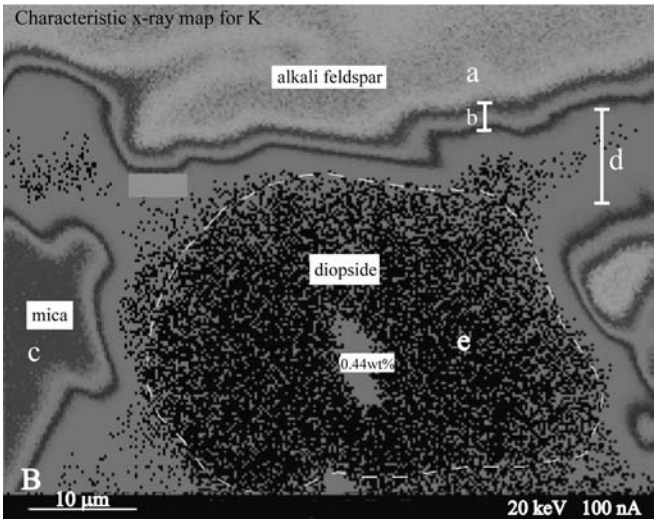

Fig. 4 BSE images showing K-clinopyroxene micro-inclusions in diopside host. **A** and **B** represent their chemical analyses in Table 2 (**A**); **B** characteristic X-ray map for K, obtained by an electron microprobe, showing the irregular concentration of such element in the core of a basal section of an elongate diopside. Gray scale: *a* feldspar zone with about 14 wt% of K_2O; *b* feldspar zone with K_2O ranging between 12 wt% and 9 wt%; *c* mica zone with about 9 wt% of K_2O; *d* probable zone in the contact regions of crystals with secondary fluorescence; *e* diopside with K_2O below the detection limit and core with 0.44 wt%

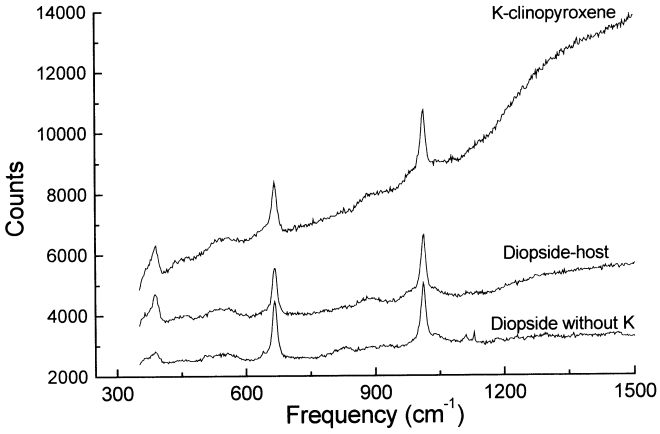

Fig. 5 Representative Raman spectra of K-clinopyroxene micro-inclusions, its diopside host, and one diopside crystal without potassium in the same sample

apfu. Both types have high TiO_2 contents, from 3 to 4 wt% (0.4–0.5 apfu). Most grains have high-F concentrations, occupying up to 50% of the hydroxyl site. Phlogopite has Na_2O contents between 0.29 and 0.33 wt% (Table 3), which are typical values of phlogopites from minette lamprophyres (Bachinski and Simpson 1984), or other lamprophyre types (Arima and Edgar 1982), camptonites (Cooper 1979), ultrapotassic lavas (Barton 1979), and shoshonitic lavas (Joplin et al. 1972). The lower K-contents of phlogopites in the mme (Table 3), suggest the exchange of K^+ by Na^+. Some Ca in the structural formulae of phlogopite is a characteristic also observed in micas from minettic lamprophyres (Rock 1991). BaO contents are frequently below the detection limit, but some grains have amounts from 0.2 to 0.4 wt%. The composition of phlogopite is close to the average composition of minette phlogopite (Bachinski and Simpson 1984), as displayed in Table 3. Mg-biotite has lower #mg than typical micas of minettes, reflecting the decreasing in the #mg of melt during crystallization, as also observed by Hall (1982) in the Pendennis minette at Falmouth, Cornwall. The latest crystallized poikilitic grains of mme, probably formed under near-solidus conditions, have lower TiO_2 contents (2.5–2.9 wt%).

The exchange schemes involve replacement of Mg by Fe^{+2} in the octahedral site (Fig. 7B), and the slight correlation of Ti and ^{VI}Al requires substitution of ^{IV}Al for Si^{+4} in the tetrahedral site for charge balance (Fig. 7C). Exchange of ^{IV}Al for Si^{+4} is also suggested for phlogopite, which is poorer in Si^{+4} and richer in ^{IV}Al than Mg-biotite.

Garnet

Garnet was only found as inclusions in pyroxene phenocrysts of mica-clinopyroxene cumulates. One grain was analyzed, but several micro-inclusions ($\ll$2 μm wide) were detected (EDS spectra) in clinopyroxene phenocrysts of the same cumulate sample. Unfortunately, the reduced size of such micro-inclusions is under the analytical capacity of electron microprobe. The analyzed garnet is weakly grayish-pink in color, with a subrounded shape. It is poor in TiO_2 (<0.1 wt%) and Cr_2O_3 (below detection limit) and is a Mg-rich, Ca-poor member of the ternary pyrope-grossular-almandine (Table 4). The Si content lower than 3.0 apfu indicates the absence of majorite [$Mg_3(MgSi)Si_3O_{12}$] component and can be related to $^{IV}Al + Na^+ + K^+$ incorporation in the garnet structure. The 100×[MgO/(MgO + FeOt)] ratio is intermediate to high, reaching values of 54, whereas the #mg is close to 68 (Table 4), which are comparable with the high

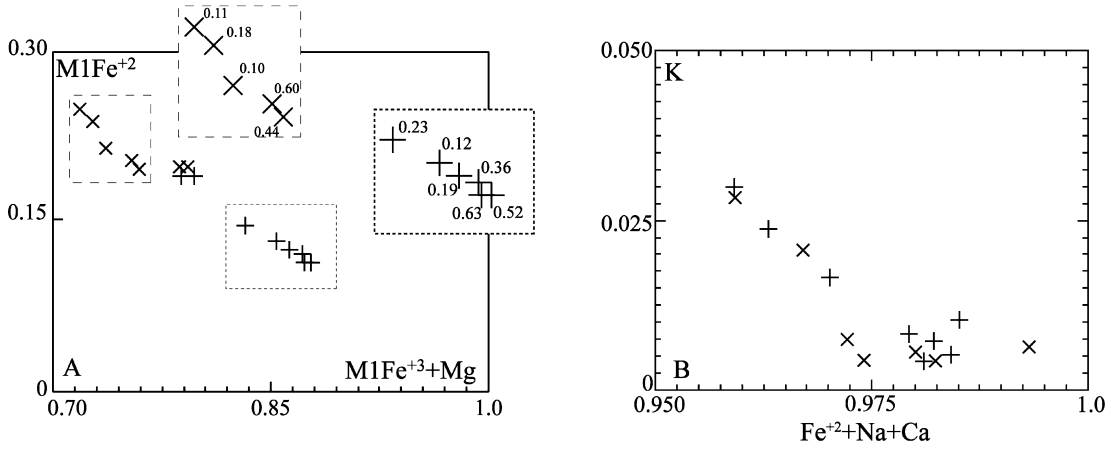

Fig. 6 Coupled substitutions in K-clinopyroxenes. (+) K-clinopyroxene phenocrysts; (*X*) K-clinopyroxene groundmass crystals. Detailed fields show the K_2O contents varying with Fe and Mg

#mg of host diopside phenocryst, around 71. The nearly similar #mg of garnet and its host pyroxene suggests equilibrium between both phases during crystallization. Using the Ca–Mg–Fe cationic parameters, this garnet has a composition enriched in pyrope component (61%), with minor amounts of andradite (25.4–27.2%) and almandine (11.3–13.2%). The low Al_2O_3 contents (1.95–1.99 apfu) require some ferric iron to fill octahedral site (Table 4). Garnet inclusions are also marked by measurable concentrations of Na_2O and K_2O, reaching up to 0.11 and 0.13, respectively.

Amphibole

Amphibole of mme and cumulates occurs as lamellae and micro-inclusions in clinopyroxene phenocrysts and rims in some clinopyroxene groundmass crystals, and their composition, according to Leake et al. (1997), range among edenite, Mg-hornblende, and actinolite (Table 4). Usually, the amphibole associated to clinopyroxene rims is actinolite (Table 4). The high alkali contents ($Na_2O + K_2O < 3.51$ wt%) are diagnostic of all these amphiboles, with the lowest contents observed in actinolite. Fluorine determinations in some grains demonstrate that all types show high contents, with not corrected F-contents reaching up to 1.46 wt% in lamellae and micro-inclusions, and 1.24 wt% in actinolite.

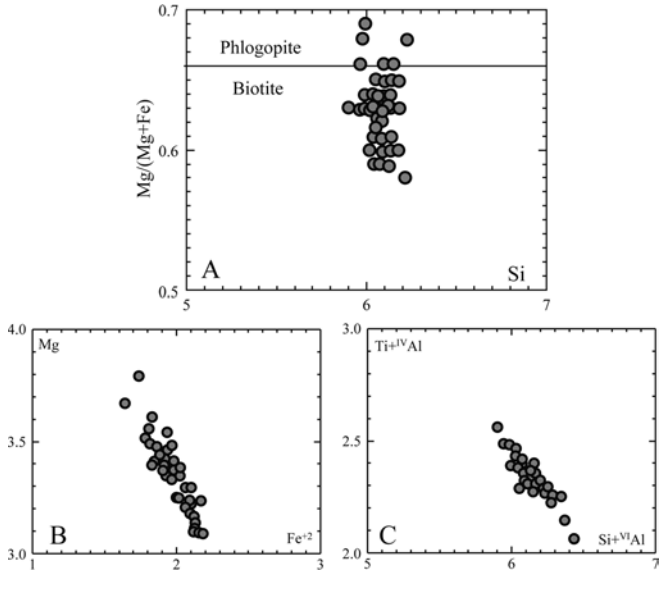

Fig. 7 Classification diagram for micas, after Rieder et al. (1998). **A** Phlogopite analyses correspond to lath inclusions in diopside; **B**, **C** substitutional scheme for micas of mme

Discussions

Chemical preservation and crystallization order of mafic magma

It is always difficult to recognize if the mafic magma in a mingling system was or not preserved of chemical change (Orsini et al. 1991; Nardi and Lima 2000). Chemical changes are accentuated by thermal and compositional differences between both magmas (Vernon 1990; Didier and Barbarin 1991). In the case of mme from Piquiri Syenite, several petrographic features indicate that in most of them chemical changes were negligible. The mme phases crystallized during the pre-mingling stage and those produced during the fast cooling stage are the same; additionally, the cumulates are composed of the same pre-mingling, early-crystallized clinopyroxene, mica, and apatite. It is concluded that no significant compositional variation was produced in the mafic magma preserved as mme, by mingling with the syenitic one. Furthermore, the lack of mica concentrations along the contacts of mafic enclaves and the host syenite, indicates that K, Rb, volatile, and water migration into the mafic magma did not occurred. Probably, the major compositional modification during mingling was the diffusion of water and other volatiles from the mafic lamprophyric magma into the syenitic one. Since both magmas probably had more or less similar compositions large chemical gradients were not established.

Table 3 Representative analyses (in wt.%) of micas of mme. *Phlg* Phlogopite; *Mg-bi* magnesian biotite, * phlogopite inclusions in clinopyroxene. Last column shows the compositional variation and average composition of phlogopites from minettes (Bachinski and Simpson 1984)

	*	*	Phlog	Phlog	Phlog	Mg-bi	Mg-bi	Mg-bi	Mg-bi	Mg-bi	Mg-bi	Mg-bi	Mg-bi	Mg-bi	Mg–bi	Minette
SiO_2	40.66	39.76	40.07	40.20	40.82	39.63	38.76	39.29	40.10	39.85	39.66	39.91	39.97	39.67	39.47	(38.4–41.7) 38.6
TiO_2	3.67	3.40	3.56	3.34	3.73	3.39	3.39	3.07	3.31	2.48	3.80	3.61	3.72	3.61	3.47	(1.4–11.3) 4.5
Al_2O_3	11.95	11.90	11.22	11.28	11.25	11.27	10.82	11.03	10.73	10.81	11.18	10.83	10.98	10.62	10.75	(9.7–18.0) 13.4
FeO	13.34	13.91	14.07	14.02	14.55	14.17	16.12	16.33	16.61	16.86	16.89	16.27	16.43	16.48	16.32	(4.8–13.1) 7.9
Fe_2O_3	0.00	0.00	0.00	0.00	0.00	0.00	0.00	0.00	0.00	0.00	0.00	0.00	0.00	0.00	0.00	
MnO	0.11	0.13	0.14	0.00	0.13	0.15	0.13	0.17	0.20	0.17	0.21	0.16	0.25	0.23	0.21	
MgO	16.69	16.90	15.51	15.49	15.63	14.75	13.53	14.32	13.76	13.26	13.68	13.88	14.00	13.59	13.43	(14.7–25.4) 20.5
BaO	0.00	0.11	0.00	0.00	0.00	0.00	0.00	0.00	0.00	0.00	0.23	0.10	0.00	0.00	0.00	
CaO	0.23	0.00	0.00	0.00	0.00	0.00	0.00	0.00	0.00	0.12	0.10	0.00	0.00	0.00	0.00	
Na_2O	0.33	0.29	0.00	0.00	0.00	0.00	0.00	0.14	0.00	0.00	0.00	0.00	0.00	0.00	0.00	(0–1.1) 0.5
K_2O	9.43	9.23	9.83	9.99	9.98	9.71	9.56	9.79	9.74	9.78	9.44	9.42	9.82	9.88	9.60	(4.4–10.6) 9.2
F	0.87	1.41	2.13	1.08	1.15	1.14	1.10	0.99	1.08	1.16	0.89	0.93	1.20	0.97	0.98	1.11
O_F	0.40	0.66	0.90	0.45	0.50	0.48	0.49	0.44	0.45	0.51	0.40	0.39	0.53	0.43	0.44	
Total	98.54	97.86	96.53	96.35	98.19	95.06	94.32	96.19	96.44	95.37	97.23	96.18	97.27	96.12	95.27	
Structural formulae based on 23 oxygens																
Si	6.01	5.98	6.16	6.11	6.11	6.12	6.11	6.07	6.17	6.23	6.06	6.13	6.11	6.13	6.15	
^{IV}Al	2.00	2.02	1.84	1.89	1.89	1.88	1.89	1.93	1.83	1.77	1.94	1.87	1.89	1.87	1.86	
^{VI}Al	0.08	0.09	0.19	0.13	0.09	0.17	0.12	0.08	0.11	0.21	0.07	0.09	0.09	0.07	0.12	
Ti	0.41	0.39	0.41	0.38	0.42	0.39	0.40	0.36	0.38	0.29	0.44	0.42	0.43	0.42	0.41	
Fe^{2+}	1.65	1.75	1.81	1.78	1.82	1.83	2.12	2.11	2.14	2.20	2.16	2.09	2.10	2.13	2.13	
Mn	0.01	0.02	0.02	0.00	0.02	0.02	0.02	0.02	0.03	0.02	0.03	0.02	0.03	0.03	0.03	
Mg	3.68	3.79	3.55	3.51	3.49	3.40	3.18	3.30	3.15	3.09	3.12	3.18	3.19	3.13	3.12	
Ba	0.00	0.01	0.00	0.00	0.00	0.00	0.00	0.00	0.00	0.00	0.01	0.01	0.00	0.00	0.00	
Ca	0.04	0.00	0.00	0.00	0.00	0.00	0.00	0.00	0.00	0.02	0.02	0.00	0.00	0.00	0.00	
Na	0.10	0.09	0.00	0.00	0.00	0.00	0.00	0.04	0.00	0.00	0.00	0.00	0.00	0.00	0.00	
K	1.78	1.77	1.93	1.94	1.91	1.91	1.92	1.93	1.91	1.95	1.84	1.85	1.92	1.95	1.91	
Cation	15.74	15.90	15.91	15.75	15.74	15.72	15.76	15.84	15.72	15.79	15.68	15.65	15.76	15.73	15.70	
#mg	0.69	0.68	0.66	0.66	0.66	0.65	0.60	0.61	0.60	0.58	0.59	0.60	0.60	0.60	0.59	

One of most important petrogenetic aspects of the lamprophyric-syenitic mingling system is the crystallization order. The high #mg number found in clinopyroxene from cumulates indicates that they are formed of very early crystallized phases, and in this way, apatite and garnet, both occurring as inclusions in clinopyroxene, are probably crystallized close to lamprophyric magma liquidus temperatures. The presence of numerous micro-inclusions of garnet, detected by EDS analyses in clinopyroxene, and its #mg, close to that of host clinopyroxene, rules out the hypothesis that it is a mantle xenocryst. Additionally, the presence of potassium in its structure confirms the K-rich nature of its parental magma. Mg-hornblende and edenite occur as inclusions and lamellae in clinopyroxene of mme, sometimes replaced by actinolite. They probably represent transformed early magmatic phases, since amphiboles with such compositions are not expected under high-pressure conditions. Phlogopite occurs as inclusions in clinopyroxene, which indicates that it is crystallized at temperatures close to the lamprophyric magma liquidus. Minor phases such as zircon and sulphides are commonly observed as inclusions in clinopyroxene phenocrysts and so are interpreted as early-crystallized phases. Fe–Ti–oxides observed as inclusions too, are probably associated to the late generation of actinolite. A second stage of crystallization is marked by temperature decrease caused by commingling with syenitic magma. During this stage the textural changes are prominent whilst the mineralogical ones are less pronounced. Elongate and acicular diopside, magnesian biotite and apatite are dominant. Alkali feldspar and poikilitic magnesian biotite grains are the latest crystallized magmatic minerals and enclose all groundmass phases. Late-magmatic or post-magmatic re-equilibrations are mainly transformations of mafic minerals to actinolite.

Constraints on the source, and thermobarometry of mme

The term lamprophyre has been usually employed to volcanic and hypabyssal rocks. Rock (1984), Bergman (1986), and Esperança and Holloway (1987) described minette-like lamprophyres occurring as sills and plugs. The association of syenites and minettes was described in Brazil: the Paleoproterozoic Cara Suja (Paim 1998) and Morro do Afonso (Rios 1998) massifs. Other examples are the Miocene province of northwest Colorado, USA (Leat et al. 1988, 1989; Thompson et al. 1989), the Archean Abitibi Greenstone Belt, Canada (Mc Neil and Kerrich 1986), and the Late Silurian Scottish dykes (Thompson and Fowler 1986). In contrast with these examples, the mafic rocks associated with Piquiri Syenite do not constitute dyke intrusions,

Table 4 Representative analyses (in wt%) of garnet (grt.) and amphibole (amp.). Garnet end members: *ad* andradite; *py* pyrope; *sp* spessartine; *al* almandine. Amphibole: *inc.amp.* amphibole inclusions in clinopyroxene phenocrysts; *lam. amp.* amphibole lamellae in clinopyroxene. Structural formulae of garnet based on 12 oxygens, and of amphibole on 23 oxygens

	grt.	grt.	grt.	grt.		inc. amp.	inc. amp.	lam. amp.	lam. amp.
SiO_2	39.852	39.625	38.463	38.748	SiO_2	47.631	47.067	51.796	54.632
TiO_2	0.000	0.000	0.000	0.000	TiO_2	0.970	0.129	0.811	0.200
Al_2O_3	15.010	14.458	14.405	14.078	Al_2O_3	6.280	6.660	3.671	1.573
FeO	7.997	7.682	8.018	7.543	FeO	14.088	14.179	11.060	12.318
Fe_2O_3	12.860	13.003	12.809	13.131	MnO	0310	0.272	0.261	0.208
MnO	0.150	0.131	0.167	0.166	MgO	14.161	13.725	16.359	16.270
MgO	23.216	22.320	22.531	22.283	CaO	11.002	10.588	11.572	10.145
CaO	0.566	0.716	0.574	0.624	Na_2O	2.411	2.744	1.885	2.099
Na_2O	0.000	0.000	0.105	0.109	K_2O	0.708	0.768	0.536	0.486
K_2O	0.000	0.113	0.112	0.125	F	0.480	0.514	n.d.	n.d.
Total	99.650	98.050	97.180	96.810	Total1	98.050	97.810	97.990	97.930
FeOt	19.569	19.382	19.544	19.358	O = F	0.200	0.220	–	–
Si	2.938	2.969	2.920	2.948	Total2	97.850	97.590	97.990	97.930
Ti	0.000	0.000	0.000	0.000	Si	6.964	6.919	7.433	7.773
Al	1.311	1.283	1.295	1.269	Ti	0.107	0.143	0.088	0.021
Fe^{2+}	0.493	0.481	0.509	0.480	Al	1.082	1.153	0.620	0.264
Fe^{3+}	0.717	0.737	0.735	0.756	Fe^{+2}	1.209	1.282	1.177	1.079
Mn	0.009	0.008	0.011	0.011	Fe^{+3}	0.514	0.461	0.150	0.387
Mg	2.551	2.493	2.550	2.527	Mn	0.038	0.034	0.032	0.025
Ca	0.045	0.058	0.047	0.051	Mg	3.087	3.008	3.500	3.451
Na	0.000	0.000	0.015	0.016	Ca	1.723	1.668	1.779	1.547
K	0.000	0.011	0.011	0.012	Na	0.684	0.782	0.525	0.579
					K	0.132	0.144	0.105	0.088
^{IV}Al	0.062	0.031	0.080	0.052	^{IV}Al	1.036	1.081	0.567	0.227
^{VI}Al	1.248	1.253	1.215	1.217	^{VI}Al	0.046	0.072	0.053	0.037
ad	25.970	26.940	26.340	27.220					
py	61.850	61.060	61.180	60.950					
sp	0.230	0.200	0.260	0.260					
al	11.950	11.790	12.220	11.950					
#mg	67.894	67.241	67.266	67.232					

since both magmas have interacted before large-scale crystallization. The main importance of mme characterization in this study is that they offer an opportunity to characterize minette-like magmas chilled at high pressures.

Several works dealing with experimental and geochemical data, or with mantle xenoliths obtained from minette magmas are in agreement on their probable lithospheric mantle source and on their primary composition (Ehrenberg 1979; Bachinski and Simpson 1984; Esperança and Holloway 1987; Leat et al. 1988; Thompson et al. 1989; Gibbson et al. 1993). However, little experimental data on stability mineral of minettic primary melts exists (Esperança and Holloway 1987). The most interesting and useful model to explain the differences between the large spectrums of K-rich rocks is that created by Foley (1992). In this model phlogopite-amphibole-diopside-rich veins crosscut peridotitic or harzburgitic mantle host, and melting is induced by the addition of incompatible and volatile elements. The initially strong alkaline melts in vein assemblages become diluted by peridotitic or harzburgitic components from the wall rocks, in the most advanced melting stages. Hence, most of vein-derived melts are hybrid and their composition depends on the proportion of melted vein/wall rock. This model was developed in order to explain the origin and chemical composition of lamproitic melts. However, depending on the melting stage and mineral composition of the vein assemblage, a large spectrum of primary melts can be formed, mainly lamproitic liquids as predicted by Mitchell (1995). Mitchell and Bergman (1991) observed that in the lamprophyre clan, only minettes resemble chemically and mineralogically some lamproites.

Minettes are lamprophyric rocks that are chemically and tectonically not very different from lamproites, and Bachinski and Scott (1979) and Scott (1979) proposed the petrogenetic link between these groups of ultrapotassic rocks. Mme samples from the Piquiri Syenite were compared with minettes from Buell Park, Arizona, from Navajo Province, Colorado, and with the average composition of 42 phlogopite lamproites from Leucite Hills, Wyoming (Table 5). The most significant differences are the higher #mg, TiO_2, and K_2O contents of lamproites, whereas minettes are CaO and Na_2O enriched. Using Foley's (1992) model, the potassium-rich character of magmas produced by vein assemblage is due to phlogopite melting. However, for yielding the extremely high K_2O contents of lamproites, an additional K-bearing phase or phases are required, which according to Mitchell (1995) are K-richterite and, depending upon the pressure, K-Ti-silicates and

Table 5 Representative chemical analyses (in wt%) of mme and cumulate rocks (*). (PQ samples; Vieira et al 1989). Lamproite analyses represents the average of 42 samples from Leucite Hills (Mitchell 1995), and minette analyses from Navajo Province (Gibbson et al 1993) and from Buell Park locality (Esperança and Holloway 1987)

Sample	Fpq35 *	P211	P205	PQ06	PQ07	PQ26	PQ36	PQ41	PQ37	PQ39A	PQ39B	Lamp.	Navajo Prov.	Buell Park
SiO_2	45.72	55.36	53.43	55.83	55.25	55.85	55.58	52.93	52.82	52.83	50.32	54.51	53.67	49.13
TiO_2	1.44	0.88	1.13	0.97	0.88	1.14	0.87	0.90	0.94	1.10	1.17	2.48	1.67	2.02
Al_2O_3	4.50	12.10	12.26	13.31	12.86	13.56	12.40	12.34	12.94	11.41	10.08	10.22	11.23	10.51
Fe_2O_3	12.34	6.84	7.54	1.65	1.13	1.16	1.48	2.90	2.36	3.72	3.29		7.10	
FeO				4.60	4.40	4.55	4.49	4.10	3.94	5.75	6.55	3.78		7.80
MgO	11.57	5.56	6.36	6.60	6.83	6.02	6.81	6.83	6.90	7.39	7.32	7.61	8.20	9.87
CaO	15.79	6.50	5.80	6.08	6.43	5.01	5.39	6.83	6.30	7.48	8.15	4.33	7.64	9.06
Na_2O	1.13	2.77	2.47	3.10	2.97	3.24	3.10	3.10	3.10	2.70	2.83	1.34	1.85	2.06
K_2O	2.57	7.27	7.80	6.14	5.96	6.75	6.78	6.23	6.45	5.93	5.67	11.59	7.19	4.86
P_2O_5	2.64	1.17	1.22	1.40	1.20	0.97	1.04	1.57	1.35	1.79	2.17	1.64	1.01	0.97
$H2O^-$				0.30	0.30	0.09	0.16	0.36	0.96	0.42	0.34			
LOI	0.87	0.53	0.89	0.82	0.75	0.79	1.09	1.06	1.40	0.03	0.96		0.61	
Total	98.81	99.11	99.02	100.80	98.96	99.13	99.19	99.15	99.46	100.55	98.85	97.5	100.11	96.28
Fe_2O_3T	12.34	6.84	7.54	6.76	6.02	6.22	6.47	7.46	6.74	10.11	10.57	4.20	7.10	8.67
FeOT	11.11	6.15	6.78	6.08	5.42	5.59	5.82	6.71	6.06	9.10	9.51	3.78	6.39	7.80
#mg				53	55	51	54	53	53	50	46	61	50	50

K-feldspar. The lower K_2O contents of minettes suggest a lower contribution of phlogopite or other K-rich phases during mantle-source melting and, the higher CaO and Na_2O contents point out to larger contributions of clinopyroxene. Derivation of minette magmas from a mica-clinopyroxene-rich source is supported by the experimental studies of Lloyd et al.(1985) which demonstrated that the produced melts are ultrapotassic, with up to 6 wt% of K_2O, #mg around 60, and low Cr and Ni. Such compositional features are quite similar to those of the minettes from Piquiri Syenite, particularly the moderate #mg and the low Cr and Ni contents (Table 5). A Cr depleted-source is suggested also by its low contents determined in clinopyroxene and garnet.

Previous thermobarometry data on minette magmas, based on garnet peridotite xenoliths from Navajo minettes (Ehrenberg 1979, 1982) and diopside xenocrysts in Ship Rock Minette (Mercier 1976) pointed out to temperatures around 1,100–1,200 °C and P≅4.2 GPa for their generation. Phase assemblage experiments on minette crystallization explain the absence of garnet as the result of initial crystallization below 1–2 GPa (Esperança and Holloway 1987). Since the mafic magma from Piquiri Syenite crystallized garnet as a liquidus phase, higher–pressure experiments on K-rich systems will be considered. In all high-pressure studies concerning K-rich systems, garnet is a stable phase at higher pressures (at T = 1,200–1,300 °C; P > 5 GPa, Edgar and Vukadinovic 1993; Mitchell 1995; P > 6 GPa, Sudo and Tatsumi 1990; P > 7.5 GPa, Luth 1997; Konzett 1997). Then, the presence of pyrope as near-liquidus phase in the minette magma from Piquiri Syenite indicates early crystallization at lithospheric mantle conditions, probably under higher pressures than those proposed by Ehrenberg (1979, 1982). Phlogopite, according to the experiments cited above, would crystallize in the mafic magma at temperatures between 1,200 – 1,300 °C.

Constraints on mineral composition

Garnet with high-pyrope component is an important constituent of the upper mantle (Ohtani et al. 1981; Irifune and Ohtani 1986; Herzberg and Gasparik 1991; Mitchell 1995; Konzett 1997). Furthermore, the presence of Na in garnet is attributed to high-pressure during crystallization (Sobolev and Lavretev 1971; Moore and Gurney 1989; Mitchell 1995; Konzett 1997; Liou et al. 1998). Garnet with similar composition to those found in cumulates from Piquiri Syenite, was synthesized at high-pressure experiments on lamproitic compositions (Mitchell 1995) and coesite-bearing eclogite (Okamoto and Maruyama 1998). In both cases, the Na_2O concentrations around 0.1 wt% obtained at 5 GPa, are the same as those of Piquiri cumulates. Similar Na_2O contents are reported in garnets from eclogite suites, as inclusions in diamonds (Sobolev and Lavretev 1971; Moore and Gurney 1989). In our opinion, and based on previous data of Konzett (1997), the measurable K_2O concentrations in garnet are an additional argument for its very high pressure of crystallization. However, the scarcity of additional data about potassium in garnet precludes any correlation between concentration and pressure estimations.

The main carriers of Ti in mme are phlogopite and magnesian biotite, both with similar contents (Table 3). The similar Ti-contents in inclusions, phenocrysts, and elongate groundmass mica crystals suggest that this element activity was not affected by mingling. Considering the TiO_2 average contents of 0.99 wt% in mme, the mean of partition coefficient for TiO_2 ($^{mica/rock}D_{TiO2}$) is around 3.5 for both phlogopite and magnesian biotite. High fO_2 condition (Arima and Edgar 1982; Bachinski and Simpson 1984) and high temperatures (Barton and Hamilton 1982) increase the partition of Ti into mica. According to Bachinski and Simpson (1984), most of

Ti-rich phlogopite in minettic system crystallizes at fO_2 between the NNO–HM buffers, and the data of Esperança and Holloway (1987) showed an increase in $^{mica/rock}D_{TiO2}$ (at P = 1.5 GPa and T = 1,080 °C) of 1.64 (IW buffer) to 2.27 (NNO buffer). The higher $^{mica/rock}D_{TiO2}$ of mme, about 3.5, suggests higher fO_2 conditions than those reported by Esperança and Holloway (1987), considering similar temperatures of crystallization.

Cumulates of Piquiri Syenite contain clinopyroxene with the highest observed #mg, comparable to some of mme phenocrysts. Together with the presence of garnet inclusions, which are considered to be a liquidus phase, these rocks include high-pressure minerals crystallized in the lamprophyric magma. Effectively, the difference between #mg of cumulate clinopyroxenes and those of inclusions in alkali feldspar oikocrysts confirms that most cumulate minerals are not in equilibrium with their interstitial magma. However, the similarity of early-crystallized minerals in mme, of inclusions in alkali feldspar oikocrysts, and of cumulate components, indicates their co-magmatic character.

In spite of K contents in clinopyroxene are directly related to pressure increase (Harlow and Veblen 1991; Edgar and Vukadinovic 1993, and many others), Harlow (1997) synthesized K-rich pyroxenes at very high pressures (up to 14 GPa) observing invariable $^{cpx/rock}D_{K2O}$. In this way, considering that K-rich micro-inclusions are crystallized from the mafic magma at the initial stages of co-mingling, as suggested by its shape (Fig. 4A), the strongly K-enriched compositions probably reflect crystallization at high pressure but under non-equilibrium conditions. Most of K-rich clinopyroxenes exhibit $^{cpx/melt}D_{K2O}$ between 0.03 and 0.12 (Edgar and Vukadinovic 1993; Mitchell 1995; Harlow 1997). In the case of the lamprophyric magma of the Piquiri Syenite it is difficult to estimate melt composition, and the partition of K is represented by $^{cpx/rock}D_{K2O}$. Certainly, K-rich zones analyzed in the core of some phenocrysts (Table 2) crystallized in equilibrium with the lamprophyric magma, and using the K_2O contents of sample P–211 (Table 5), which contains the K-rich phenocrysts, the calculated $^{cpx/rock}D_{K2O}$ range from 0.015 to 0.087. Although the elongate groundmass crystals were developed during mingling, it is not clear if the K-rich cores (Fig. 4B) crystallized before or during chilling. So, it is difficult to prove that such clinopyroxene cores are really in equilibrium with melt, although $^{cpx/rock}D_{K2O}$ of these elongate groundmass crystals is in the range observed for K-rich phenocrysts. In order to compare the observed $^{cpx/rock}D_{K2O}$ data with experimental $^{cpx/melt}D_{K2O}$ values of Edgar and Vukadinovic (1993) and Mitchell (1995) all analytical points were plotted in Fig.8. It seems clear that phenocryst cores with high K contents crystallized at 4–6 GPa and 1,200–1,300 °C. Although this direct interpretation is limited by probable differences between K_2O contents of parental melt and mme, such data are supported by the contents of Na^+ found in the garnet inclusion. In any case, the major point is not to determine the crystallization pressure of K-clinopyroxenes, but to show that such K was incorporated by clinopyroxene at lithospheric mantle conditions, and was preserved due to mingling-promoted chilling of the minettic magma. Acicular K-rich clinopyroxene micro-inclusions and K-rich cores of several groundmass elongate grains analyzed in several samples support this hypothesis. Taking into account the preservation of K-clinopyroxenes, the textural evidence of chilling and, the presence of K-clinopyroxene inclusions in diopside from Piquiri Syenite, with K_2O contents from 0.12 to 0.46 wt%, it is admitted that mingling started at high pressure, still in the lithopheric mantle.

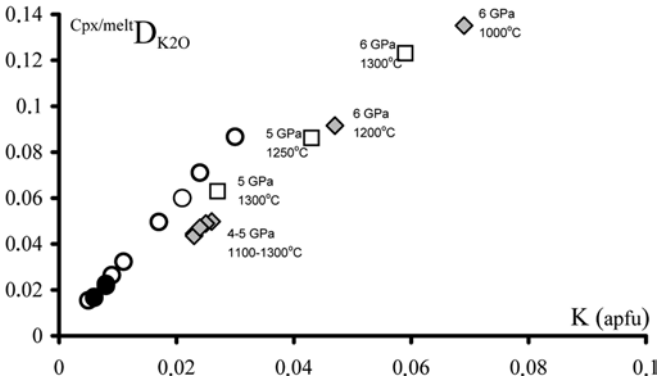

Fig. 8 $^{cpx/melt}D_{K2O}$ *vs.* K (apfu) diagram with K-clinopyroxene analyses of phenocrysts (*open circles*) and groundmass crystals core (*filled circles*), compared with those obtained in similar pyroxenes by Edgar and Vukadinovic (1993, squares), and Mitchell (1995; filled diamond)

Acknowledgements This work was supported by Fundação de Amparo a Pesquisa no Estado do Rio Grande do Sul (FAPERGS-proc. no. 99/60012-2) and PRONEX. J.P.C. thanks the Conselho Nacional de Pesquisa Científica (CNPq) for the financial support (Proc.—200767/00-3) and Xavier Llovet from Serveis Cientificotècnics (Universitat de Barcelona) for support in acquiring electron data. This manuscript was much improved by two anonymous reviewers.

References

Arima M, Edgar AD (1982) Substitution mechanism and solubility of titanium in phlogopites from rocks of probable mantle origin. Contrib. Mineral Petrol 77:288–295

Bachinski SW, Scott RB (1979) Rare-earth and other trace element contents and the origin of minettes (mica-lamprophyres). Geochim Cosmochim Acta 43:93–100

Bachinski SW, Simpson EL (1984) Ti-phlogopites of the Shaw's Cove minette: a comparison with micas of other lamprophyres, potassic rocks, kimberlites, and mantle xenoliths. Am Mineral. 69:41–56

Barbarin B (1988) Field evidence for successive mixing and mingling between Piolard Diorite and the Saint-Julien-la-Vêtre Monzogranite (Nord-Forez, Massif Central, France). Can J Earth Sci 25:49–59

Barbarin B (1990) Plagioclase xenocrysts and mafic magmatic enclaves in some granitoids of the Serra Nevada Batholith, California. J Geophys Res 95:17747–17756

Barton M (1979) A comparative study of some minerals occurring in the potassium-rich alkaline rocks of Leucite Hills, Wyoming,

the Vico Volcano, western Italy, and the Toro-Ankole region, Uganda. Neues Jahrb Mineral 137:113–134
Barton M, Hamilton DL (1982) Water-undersaturated melting experiments bearing upon the origin of potassium-rich magmas. Mineral Mag 45:267–278
Bergman SC (1986) Lamproites and other potassium–rich igneous rocks: a review of their occurrence, mineralogy and geochemistry. In: Proceedings of the Conference on Alkaline Igneous Rocks. Edinburgh
Bittencourt MF, Nardi LVS (2000) Tectonic setting and sources of magmatism related to the Southern Brazilian Shear Belt. Rev Bras Geoc 30(1–3). CD-version
Bukowinski MST, Knopoff L (1977) Physics and chemistry of iron and potassium at lower-mantle and core pressures. In: Manghani MH, Akimoto S (eds) High-pressure research applications in geophysics. Acaddemic Press, New York, pp 367–388
Collerson KD, Hapugoda S, Kamber BS, Williams Q (2000) Rocks from the Mantle Transition Zone: majorite-bearing xenoliths from Malaita, southwest Pacific. Science 288**:**1215–1223
Cooper AF (1979) Petrology of ocellar lamprophyres from western Otago, New Zealand. J Petrol 20:139–163
Didier, J., Barbarin, B (1991) Enclaves and granite petrology. Elsevier, Amsterdam, 625 pp
Droop GTR (1987) A general equation for estimating Fe^{+3} concentrations in ferromagnesian silicates and oxides from microprobe analyses using stoichiometric criteria. Mineral Mag 51:431–435
Edgar AD, Vukadinovic D (1993) Potassium-rich clinopyroxene in the mantle: Na experimental investigation of a K-rich lamproites up to 60 Kbar. Geochim Cosmochim Acta 57:5063–5072
Ehrenberg SN (1979) Garnatiferous ultramafic inclusions in minette from the Navajo volcanic field. In: Boyd FR, Meyer HOA (eds)The mantle sample: inclusions in kimberlites and other volcanics. American Geophysical Union, Washington, DC, pp 330–344
Ehrenberg SN (1982) Petrogenesis of garnet lherzolite and megacrystalline nodules from the Tumb, Navajo volcanic field. J Petrol 23:507–547
Erlank AJ, Kushiro I (1970) Potassium contents of synthetic pyroxenes at high temperatures and pressures. Carnegie Inst Wash Yearbook 68:23–236
Esperança S, Holloway JR (1987) On the origin of some mica-lamprophyres: experimental evidence from a mafic minette. Contrib Mineral Petrol 95:207–216
Foley, SF (1992) Vein-plus-wall-rock melting mechanisms in the lithosphere and the origin of potassic alkaline magmas. Lithos 28:435–453
Gibbson AS, Thompson RN, Leat PT, Morrison MA, Hendry GL, Dickin AP, Mitchell JG (1993) Ultrapotassic magmas along the flanks of the Oligo-Miocene Rio Grande Rift, USA: monitors of the zone of lithospheric mantle extension and thinning beneath a continental rift. J Petrol 34:187–228
Hall A (1982) The Pendennis peralkaline minette. Mineral Mag 45:257–266
Harlow, GE (1996) Structure refinement of a natural K-rich diopside: The effect of K on the average structure. Am Mineral 81:632–638
Harlow GE (1997) K in clinopyroxene at high pressure and temperature: An experimental study. Am Mineral 82:259–269
Harlow GE, Veblen BR (1991) Potassium in clinopyroxenes: Inclusions from diamonds. Science 251:652–655
Harlow GE (1999) Interpretation of Kcpx and CaEs in clinopyroxene from diamond inclusions and mantle samples. In: Gurney JJ, Gurney JL, Pascoe MD, Richardson SH (eds) Proceedings of 7th International Kimberlite Convention. Redroof Desing Cc, Cape Town, 1, pp 321–331
Hartmann LA, Nardi LVS, Formoso MLL, Remus MVD, Lima EF, Mexias SA (1999) Magmatism and metallogeny in the crustal evolution of Rio Grande do Sul Shield, Brazil. Pesquisas 26(2):5–63
Herzberg C, Gasparik T (1991) Garnet and pyroxenes in the mantle: a test of the majorite fractionation hypothesis. J Geophys Res 96(B10):16263–16274
Hibbard MJ (1981) The magma mixing origin of mantled feldspars. Contrib Mineral Petrol 76:158–170
Huang R, Chen CH, Lin EH, Xu JA (2000) Raman spectroscopic characteristics of Mg–Fe–Ca pyroxenes. Am Mineral 85:473–479
Irifune T, Ohtani E (1986) Melting of pyrope $Mg_3Al_2Si_3O_{12}$ up to 10 GPa: possibility of a pressure-induced structural change in pyrope melt. J Geophys Res 91(B9):9357–9366
Joplin GA, Kiss E., Ware NH, Widdowson JR (1972) Some chemical data on members of the shoshonite association 38:936–945
Konzett J (1997) Phase relation and chemistry of Ti-rich K-richterite-bearing mantle assemblages: an experimental study to 8.0 GPa in a Ti-KNCMASH system. Contrib Mineral Petrol 128:385–404
Kudoh Y, Prewitt CT, Finger LW, Ito E (1992) Ionic-bound strength systematics, ionic compressibilities and an application to (Mg, Fe)SiO_3 perovskites. In: Syono Y, Manghnani MH (eds) High-pressure research: applications to earth and planettary sciences. American Geophysical Union, Washington, DC, pp 215–218
Le Maitre RW (1989) A classification of igneous rocks and glossary of terms. Blackwell, Oxford. 193 pp
Leake BE, Wooley AR, Arps CES, Birch WD, Gilbert MC, Grice JD, Hawthorne FC, Kato A, Kisch HJ, Krivovichev VG, Linthout K, Laird J, Mandarino JÁ, Maresch WV, Nickel EH, Rock NMS, Schumacher JC, Smith DC, Stephenson NCN, Ungaretti L, Whittaker EJW, Youzhi G (1997) Nomenclature of amphiboles: report of the subcommittee on Amphiboles of the International Mineralogical Association, Commission on New Minerals and Mineral Names. Am Mineral 82:1019–1037
Leat PT, Thompson RN, Dickin MA, Morrison MA, Hendry GL (1988) Quaternary volcanism in northwestern Colorado: implications for the roles os asthenosphere and lithosphere in the genesis of continental basalts. J Volcanol Geotherm Res 37:291–310
Leat PT, Thompson RN, Morrison MA, Hendry GL, Dickin MA (1989) Silicic magmas derived by fractional crystallization from Miocene minettes, Elkhead Mountains, Colorado. Mineral Mag 52:577–585
Lima EF, Nardi LVS (1998) The Lavras do Sul Shoshonitic Association: implications for the origin and evolution of Neoproterozoic shoshonitic magmatism in southernmost Brazil. J S Am Earth Sci 11(1):67–78
Liou JG, Zhang RY, Ernst WG, Rumble D, Maruyama S (1998) High pressure minerals from deeply subducted metamorphic rocks. In: Hemley RJ (ed) Ultra high-pressure mineralogy: physics and chemistry of the Earth's deep interior. Rev Mineral Mineral Soc Am 37:33–96
Loyd FE, Arima M, Edgar AD (1985) Partial melting of a phlogopite cliopyroxenite nodule from southwest Uganda: an experimental study bearing on the origin of highly potassic continental rift volcanics. Contrib Mineral Petrol 91:321–329
Luth RW (1992) Potassium in clinopyroxene at high pressure: experimental constraints (abs.) EOS 73:608
Luth RW (1997) Experimental study of the system phlogopite-diospide from 3.5 to 17 GPa. Am Mineral 82:1198–1209
McMillan P (1989) Raman spectroscopy in mineralogy and geochemistry. Annu Rev Earth Planet Sci 17:255–283
McNeil AM, Kerrich R (1986) Archean lamprophyres dykes and gold mineralizations, Matheson, Ontario: the conjunction of REE-enriched mafic magmas, deep crustal structures and Au concentrations. Can J Earth Sci 23:324–33
Mercier J-C (1976) Single-pyroxene geothermometry and geobarometry. Am Mineral 61:603–615
Mernagh TP, Hoatson DNJ (1997) Raman spectroscopic study of pyroxene structures from the Munni Munni layered intrusion, Western Australia. J Raman Spectrosc 28(9):647–658

Mitchell RH (1995) Melting experiments on a sanidine phlogopite lamproite at 4–7 GPa and their bearing on the sources of lamproitic magmas. J Petrol 36(5):1455–147

Mitchell RH, Bergman SC (1991) Petrology of lamproites. Plenum Press, New York, 447 pp

Montford CE, Swanson CA (1965) An experimental equation of state of potassium metal. Phys Chem Solids 26:291–301

Moore RO, Gurney JJ (1989) Mineral inclusions in diamonds from the Monastery kimberlite, South Africa. In: Ross J (ed) Proceedings of the 4th International Kimberlite Conference, Kimberlites and Related Rocks. vol 2. Their Mantle/Crust Setting, Diamonds and Diamond Exploration. Spec Publ, Geol Soc Aust 14:1029–1041

Morimoto CN (1988) Nomenclature of pyroxenes. Mineral Mag 52:535–550

Nardi LVS, Lima EF (1985) The Lavras do Sul Shoshonitic Association, RS. (A Associação Shoshonítica de Lavras do Sul, RS). Rev Bras Geoc 15:139–16

Nardi LVS, Lima EF (2000) Hybridisation of mafic microgranular enclaves in the Lavras Granite Complex, southern Brazil. J S Am Earth Sci 13:67–78

Ohtani E, Irifune T, Fujino K (1981) Fusion of pyrope at high pressure and rapid crystal growth from the pyrope melt. Nature 294:62–64

Okamoto K, Maruyama S, (1998) Multi-anvil re-equilibration experiments of a Dabi Shan ultra high-pressure eclogite within the diamond-stability fields. Island Arc 7:52–69

Orsini JB, Cocirta C, Zorpi MJ (1991) Genesis of mafic microgranular enclaves through differentiation of basic magmas, mingling and chemical exchanges with their host granitoid magmas. In: Didier J, Barbarin B (eds) Enclaves and granite petrology. Elsevier, Amsterdam, pp 445–464

Paim MM (1998) Petrology of the Cara Suja Potassic Syenite, south-western Bahia (Petrologia da Intrusão Sienítica Potássica de Cara Suja, Sudoeste da Bahia). In: Conceição H, Cruz MJM (eds) Paleoproterozoic Alkaline potassic and ultrapotassic syenites from Bahia State (Sienitos Alcalino-Potássicos e Ultrapotássicos Paleoproterozóicos do Estado da Bahia). SBG publicação especial no 4, Salvador, Brasil, pp 111–141

Plá Cid J, Nardi LVS, Conceição H, Bonin B (2000) Mineralogical and geochemical discrimination between K-rich syenites in northeastern Brazil. 31st International Geological Congress, Rio de Janeiro, Abstracts Volume

Plá Cid J, Nardi LVS, Enrique P (2002) Textural relations of lamprophyric mafic microgranular enclaves and petrological implications for the genesis of potassic syenitic magmas: the example of Piquiri Syenite, southern Brazil. Pesq em Geoc (in press)

Rieder M, Cavazzini G, D'Yakonov YS, Frank-Kamenetskii VA, Gottardi G, Guggenheim S, Koval PV, Muller G, Neiva AMR, Radoslovich EW, Robert J-L, Sassi FP, Takeda H, Weiss Z, Wones DR (1998). Nomenclature of micas. Can Mineral 36(3):905

Rios DC (1998) Petrology of the potassic-ultrapotassic and lamprophyric magmatism from Morro do Afonso—Bahia (Petrologia do Magmatismo Potássico-Ultrapotássico e Lamprofírico de Morro do Afonso—Bahia). In: Conceição H, Cruz MJM (eds) Paleoproterozoic alkaline potassic and ultrapotassic syenites from Bahia State (Sienitos Alcalino-Potássicos e Ultrapotássicos Paleoproterozóicos do Estado da Bahia). SBG publicação especial no 4, Salvador, Brasil, pp 167–204

Rock NMS (1984) Nature and origin of calc-alkaline lamprophyres: minettes, vogesites, kersantites, and spessartites. Trans R Soc Edinb 74:193–227

Rock NMS (1991) Lamprophyres. Blackie-Van Norstrand Reinhold, New York. 285 pp

Scott BH (1979) Petrogenesis of kimberlites and associated potassic lamprophyres from central west Greenland. In: Boyd FR, Meyer HOA (eds) Kimberlites, diatremes, and diamonds: their geology, petrology, and geochemistry. American Geophysical Union, Washington, DC, pp 190–205

Sobolev NV, Lavretev YG (1971) Isomorphic sodium admixture in garnets formed at high pressures. Contrib Mineral Petrol 31:1–12

Sobolev NV, Zueo VM, Bezburodov SM, Aononarenko AI, Spetsius ZV, Kuligin S, Yefinova ES, Afanasiev VP, Koptil VI, Bolikinov, AL (1991) Eclogite paragenesis of diamonds from Udachnaya and Mir pipes, Yakutea. 5th International Kimberlite Conference, Abstract Volume

Sobolev NV, Shatsky VS, Vavilov MA, Goryainov SV (1994) Zircons from ultra high pressure metamorphic rocks of folded regions as unique container of inclusions of diamond, coesite and coexisting minerals. Dokl Akadi Nauk 334:488–492

Sudo A, Tatsumi Y (1990) Phlogopite and K-amphibole in the upper mantle: implication for magma genesis in subduction zones. Geophys Res Lett 17:29–32

Thompson RN, Fowler MB (1986) Subduction-related shoshonitic and ultrapotassic magmatism: a study of Siluro-Ordovician syenites from the Scottish Caledonides. Contrib Mineral Petrol 94:507:522

Thompson RN, Morrison MA, Hendry GL, Parry SJ (1984) Na assessment of the relative roles of crust and mantle in the magma genesis: an elemental approach. Philos Trans R Soc Lond A310:549–590

Thompson RN, Leat PT, Dickin AP, Morrison MA, Hendry GL, Gibson SA (1989) Strongly potassic mafic magmas from lithospheric mantle sources during continental extension and heating: evidence from Miocene minettes of northwest Colorado, U.S.A. Earth Planet Sci Lett 98:139–153

Vernon RH (1983) Restite, xenoliths and microgranitoid enclaves in granites. J Proc Soc N S W 116:77–103

Vernon RH (1990) Crystallization and hybridism in microgranitoid enclaves magmas: microstructural evidence. J Geophys Res 95:1789–17859

Vernon RH (1991) Interpretation of microstructures of microgranitoid enclaves. In: Didier J, Barbarin B (eds) Enclaves and granite petrology. Elsevier, Amsterdam, pp 277–290

Viera N Jr, Fernandes LAD, Koester E, Sherer CS (1989) Microgranular enclaves from Piquiri Syenitic massif, RS (Enclaves microgranulares do maciço sienítico de Piquiri-RS). Acta Geol Leop 29:185–206

Wang A, Jolliff BL, Haskin LA, Kuebler KE, Viskupic KL (2001) Characterization and comparison of structural and compositional features of planetary quadrilateral pyroxenes by Raman spectroscopy. Am Mineral 86:790–806